The Journal of Chemical Physics

Heat-induced degradation of fibrils: Exponential vs logistic kinetics

Cite as: J. Chem. Phys. **152**, 115101 (2020); https://doi.org/10.1063/1.5144305
Submitted: 05 January 2020 . Accepted: 27 February 2020 . Published Online: 16 March 2020

Nguyen Truong Co, Pham Dang Lan, Pham Dinh Quoc Huy, and Mai Suan Li

AIP Publishing

The Journal of Chemical Physics ARTICLE scitation.org/journal/jcp

Heat-induced degradation of fibrils: Exponential vs logistic kinetics

Cite as: J. Chem. Phys. 152, 115101 (2020); doi: 10.1063/1.5144305
Submitted: 5 January 2020 • Accepted: 27 February 2020 •
Published Online: 16 March 2020

Nguyen Truong Co,[1] Pham Dang Lan,[2,3] Pham Dinh Quoc Huy,[1] and Mai Suan Li[1,a)]

AFFILIATIONS

[1]Institute of Physics, Polish Academy of Sciences, Al. Lotnikow 32/46, 02-668 Warsaw, Poland
[2]Institute for Computational Science and Technology, SBI Building, Quang Trung Software City, Tan Chanh Hiep Ward, District 12, Ho Chi Minh City, Vietnam
[3]Faculty of Physics and Engineering Physics, VNUHCM-University of Science, 227, Nguyen Van Cu Street, District 5, Ho Chi Minh City, Vietnam

[a)]**Author to whom correspondence should be addressed:** masli@ifpan.edu.pl

ABSTRACT

The degradation of fibrils under the influence of thermal fluctuations was studied experimentally by various groups around the world. In the first set of experiments, it was shown that the decay of fibril content, which can be measured by the ThT fluorescence assay, obeys a bi-exponential function. In the second series of experiments, it was demonstrated that when the monomers separated from the aggregate are not recyclable, the time dependence of the number of monomers belonging to the dominant cluster is described by a single-exponential function if the fraction of bound chains becomes less than a certain threshold. Note that the time dependence of the fraction of bound chains can be measured by tryptophan fluorescence. To understand these interesting experimental results, we developed a phenomenological theory and performed molecular simulation. According to our theory and simulations using the lattice and all-atom models, the time dependence of bound chains is described by a logistic function, which slowly decreases at short time scales but becomes a single exponential function at large time scales. The results, obtained by using lattice and all-atom simulations, ascertained that the time dependence of the fibril content can be described by a bi-exponential function that decays faster than the logistic function on short time scales. We have uncovered the molecular mechanism for the distinction between the logistic and bi-exponential behavior. Since the dissociation of the chain from the fibrils requires the breaking of a greater number of inter-chain contacts as compared to the breaking of the beta sheet structure, the decrease in the number of connected chains is slower than the fibril content. Therefore, the time dependence of the aggregate size is logistic, while the two-exponential behavior is preserved for the content of fibrils. Our results are in agreement with the results obtained in both sets of experiments.

INTRODUCTION

Protein aggregation is believed to be associated with neurodegenerative diseases. For example, aggregation of α-synuclein protein may be related to Parkinson's disease, while Alzheimer's disease (AD), which is often seen in older people, is presumably caused by formation of extracellular senile plaques consisting of amyloid beta (Aβ) peptides in the patient's brain.[1] Aβ peptides, which are cleaved from amyloid precursor protein (APP) under the influence of β- and γ-secretases,[2] have most abundant isoforms $A\beta_{40}$ (40 amino acids) and $A\beta_{42}$ (42 amino acids). Aβ aggregation occurs by the nucleation mechanism with the lag phase to form mature fibrils with transverse β-strands. Recent experiments have provided evidence that senile plaque levels are weakly correlated with the severity of dementia, but intermediate oligomers are predominantly toxic species.[3,4] Thus, knowledge about the intermediate stages of fibril growth plays a crucial role in determining effective AD therapy. In addition, since finite-sized oligomers and fibrils can decompose into non-toxic monomers, it is important to understand the process of dissociation in detail.

Several experimental studies of the chemical stability[5–10] and dissociation of amyloid fibrils under high pressure[11–14] and laser irradiation[15,16] have been carried out, while only a limited research was conducted to study their thermal stability.[17–24] It was shown[24]

that due to thermal fluctuations, the dissociation kinetics can be described by a bi-exponential function with two very different time scales or degradation rates.

Recently, Gruning *et al.*[25] have carried out an interesting experiment allowing for the study of the dissociation of Aβ fibrils without re-association. Using the engineered protein ZAβ3W for the sequestration of the Aβ monomer, they were able to control the dissociation by tryptophan fluorescence. The basic idea of their experiment was based on the fact that ZAβ3W inhibits the Aβ aggregation by sequestering the aggregation-prone central and C-terminal regions of the Aβ monomer.[26,27] Therefore, in the experiment of Gruning *et al.*,[25] the concurrent effect of reverse and forward reactions was avoided. More importantly, it was shown that in the absence of monomer recycling, the dissociation of fibrils obeys a single exponential law instead of bi-exponential decay. This interesting result has not been theoretically explained.

Protein aggregation, in particular, the oligomerization of full-length and truncated Aβ peptides, has been studied by many groups around the world using molecular dynamics (MD) simulation.[28–33] However, the degradation of fibrils has not been theoretically considered. On the other hand, since the destruction of insoluble amyloid fibrils is one of the possible ways to treat neurodegenerative diseases, this problem is of great interest not only from the point of view of basic research but also from the point of view of application.

In this paper, combining theory with all-atom MD and lattice-based Monte Carlo simulations, we study the temperature-driven dissociation of fibrils with and without recycling (Fig. 1). In a standard scenario with monomer recycling, the released monomer is allowed to reattach to the mother aggregate, whereas in the case without recirculation, the released monomer is removed from the studied system. We have developed an analytical theory to describe the fibril degradation with and without the capture of monomers, which are detached from the parent aggregate (we use the words aggregate and fibril with the same meaning, but, in general, the aggregate is of less order than the fibril). We showed that the time dependence of the aggregate size is described by the logistic function,

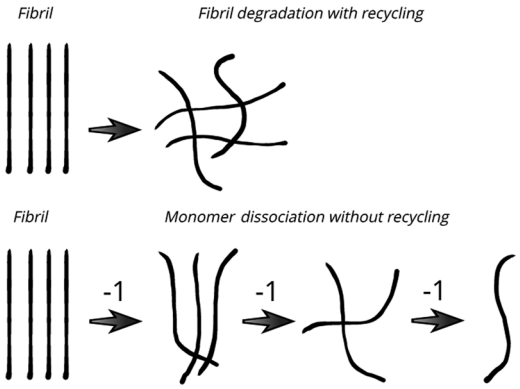

FIG. 1. Top panel: schematic plot for the dissociation of fibrils in a standard scenario with recycling, where the freed chain can reunite with the mother aggregate and, therefore, the total number of chains is fixed. Bottom panel: the decomposition of fibrils without monomer recycling, in which the released monomer is removed, not allowing to reattach to the mother unit.

while the behavior of the fibril content (the fibril content is proportional to the ThT fluorescence signal and is measured by the number of fibril contacts or beta content in simulation) is controlled by a bi-exponential function. Then, our theory and the results, obtained by tryptophan and ThT fluorescence techniques, were verified by simulations using lattice and all-atom models.

We expect that the results obtained in this work should be valid for the thermal degradation of not only proteins but also of other systems.

MATERIALS AND METHODS

Lattice model

To study the degradation of sufficiently large fibrils, we used a simple lattice model,[34,35] in which each amino acid is represented by a bead and the polypeptide chain has $M = 8$ beads. The sequence of a polypeptide chain was chosen the same as in our previous works,[34,35] i.e., this is +HHPPHH−. Here, H and P refer to hydrophobic and polar residues, respectively, while + and − are charged beads located at the ends.

The potential energy of N chains is as follows:

$$E = \sum_{l=1}^{N}\sum_{i<j}^{M} E_{sl(i)sl(j)}\delta(r_{ij}-a) + \sum_{m<l}^{N}\sum_{i,j}^{M} E_{sm(i)sl(j)}\delta(r_{ij}-a), \quad (1)$$

where the first and second terms are intra- and inter-chain interactions, respectively. r_{ij} stands for the distance between beads i and j, and the lattice spacing is denoted by a. $sm(i)$ is the type of residue i in the mth peptide, and $\delta(0) = 1$ and zero, otherwise. For intra-chain interaction, we count the interaction energy between two residues i and j that are separated by a lattice spacing but are not successive in sequence. For a cubic lattice, this condition means that $|i - j|$ must be greater or equal to 3. In the case of inter-chain interaction, any pair of two residues from different chains that are separated from each other by distance a should contribute to the interaction energy.

The energy is measured in the unit of the hydrogen bond energy ε_{HB}. We chose the contact energies as $E_{P,\alpha} = -0.2$, where α = P; +; −, and the interaction energy between two hydrophobic residues as $E_{HH} = -1$.[34] To favor the formation of "salt bridge," we assign the sufficiently strong attraction between oppositely charged beads $E_{+-} = -0.6$, while the repulsive interaction was chosen to be weaker with $E_{++} = E_{--} = -E_{+-}/2 = 0.3$. For all other contacts, we have $E_{\alpha\beta} = 0.2$. Note that the lattice model was successfully used to study the formation of critical nucleus[36] and fibril formation in a crowded environment.[37]

Monte Carlo moves

The MC (Monte Carlo) algorithm was used to study degradation of fibrils on a discrete cubic lattice. MC moves include local (corner flip, tail rotation, and crankshaft rotation) and global moves. Global moves involve translating the entire chain along a randomly chosen direction with a step of a and rotating it 90° around a randomly selected one of the three axes. Since global moves are artificial, we tried to maintain their acceptance rate as low as possible. However, if this rate is too low, the degradation process will be so slow that the problem becomes computationally unfeasible. Therefore, as in our previous work,[34] the acceptance rates of local and global moves were set at 0.9 and 0.1, respectively.

Simulation was conducted in a hypercube with a periodic boundary condition. Simulation time is measured in units of MCS (MC step), which is a combination of local and global moves.[34] The concentration of chains in each system was chosen to be around 57 μM, which corresponds to the cubic sizes of 135, 165, and 235a for N = 10, 16, and 28 monomers, respectively, with a, lattice spacing, set equal to 1. This concentration has the same order of magnitude as in typical experiments. To obtain reliable results, we performed 100–150 independent MC trajectories for each simulation set.

Fibril structures in lattice models

Fibril-like structures in the lattice model are a set of monomers forming anti-parallel structures with the lowest energy. In order to find such structures, we carried out multiple MC simulations starting from random configurations. Figure 2 shows fibril structures for N = 10, 16, and 28 for the force field described above.

Simulation of fibril degradation in lattice models

To study the kinetics and mechanisms of thermal degradation of fibrils in the lattice model, simulations were conducted starting from a fibril-like structure (Fig. 2) at various temperatures. Inter- and intra-chain contacts that exist in the fibril structure are called fibril contacts. The intra-chain contact between beads i and j is formed if $|i - j| \geq 3$, and the distance between them is equal to the lattice spacing a. The inter-chain contact between two beads belonging to two different chains occurs if the distance between them is a.

Temperature in lattice model

Since in the lattice model the energy is measured in ε_{HB}, the temperature is measured in ε_{HB}/k_B. In what follows, we use dimensionless temperature but mean that its unit is ε_{HB}/k_B. The folding temperature of the monomer T_F can be obtained either from the maximum of heat capacity[38] or from the condition $\langle Q(T_F)\rangle = 0.5$, where $Q(T_F)$ is the fraction of native contacts at the folding temperature.[34] Since the chain contains only eight beads, these quantities can be calculated exactly. From the temperature dependence of $\langle Q(T)\rangle$, we obtained $T_F \approx 0.39$ (Fig. S1 of the supplementary material). The same value of T_F was obtained from the temperature dependence of the heat capacity (results not shown). The room temperature is set as the folding temperature of the monomer $T_F = 0.39$. The lattice simulations were performed at temperatures above room temperature.

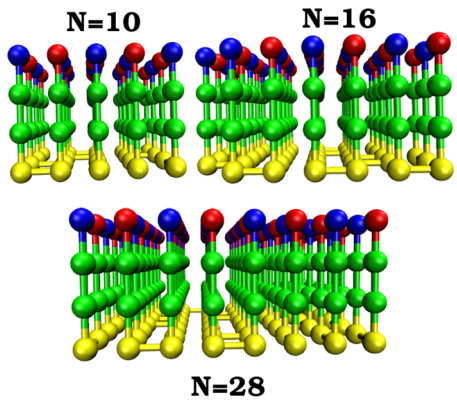

FIG. 2. Fibril structures of N = 10, 16, and 28 polypeptide chains in the lattice model. Blue, red, green, and yellow balls represent positive charges, negative charges, hydrophobic amino acids, and hydrophilic amino acids, respectively. The connections between beads are peptide bonds. These structures have 114 (84), 192 (144), and 360 (276) fibril contacts for N = 10, 16, and 28, respectively. The number of inter-chain contacts is shown in brackets.

All-atom MD simulation

The structure of Aβ fibrils remains controversial. The N-terminus of the peptide is believed to be either disordered or ordered in the fibril stage. Fibril structures of N-terminus truncated peptides were proposed by Lührs *et al.*[39] ($A\beta_{17-42}$), Petkova *et al.* ($A\beta_{9-40}$),[40] and Paravastu *et al.* ($A\beta_{9-40}$)[41] because the first 16 residues of $A\beta_{1-42}$ and the first 8 residues of $A\beta_{1-40}$ were assumed as unstructured. However, recent experiments have shown that the N-terminus might be ordered and involved in the fibril structure.[42–46] In this work, we carried out all-atom MD simulation to study the degradation of the fibril-like structure of 10 truncated peptides $A\beta_{37-42}$ (37GGVVIA42). The cross beta structure (Fig. 7) was resolved by the Eisenberg group using the solid state NMR and has ID 2ONV on the website http://people.mbi.ucla.edu/sawaya/jmol/xtalpept/index.html. We also performed the simulation for the fibril-like structure of five $A\beta_{17-42}$ chains (PDB ID: 2BEG,[39] Fig. 8).

As in the case of lattice models, the contacts formed in a fibril-like structure are called fibril contacts. The contact between two amino acids is formed if the distance between their centers of mass is less than 6.5 Å. For intra-chain contacts, we do not count the contact between successive residues.

We used the Amber11 package[47,48] to perform explicit solvent simulation applying the amber force field 99SB[49] and TIP3P water model.[50] It is worth to mention that the amber force field 99SB and TIP3P model of water is the best combination.[51,52] The motion equation was solved by the leap-frog algorithm[53] with a time step of 2 fs. By the SHAKE algorithm,[54] all bonds with hydrogen atoms were constrained. A Langevin thermostat[55] was applied to maintain the designed temperature with 2 ps^{-1} collision frequency. The vdW interaction at distances longer than 1.4 nm was not taken into account, and the electrostatic interaction was treated by the particle mesh Ewald method.[56]

Why we have to use lattice and all-atom models?

The best model to use is the all-atom model, but we also studied the lattice model for two reasons: First, due to its simplicity, we can perform simulation with a larger number of chains compared to the all-atom model. Second, in order to capture an experiment without recycling,[25] we must remove the monomer that has just dissociated from the mother aggregate before continuing with the simulation. This can be easily implemented in simple lattice models, but it is not so in an all-atom model, where the removal of one chain requires to re-solvate a simulation box with a reduced number of water molecules. In principle, to avoid this problem, we can use implicit all-atom or off-lattice coarse-grained models, but we

have chosen lattice models because they allow us to deal with a large number of polypeptide chains.

Experimental technique for monomer capture and simulation protocol

In order to prevent the released Aβ monomer itself from reuniting with the parent aggregate, experimentally it was removed from the system. For this, the free monomer was marked by the tryptophan fluorescence.[25] Since the Aβ peptide does not contain tryptophan, the ZAβ3W protein, which was obtained from ZAβ3 making a single point Y18W mutation, was used as a tryptophan fluorescence probe for monomer Aβ because it binds to the Aβ monomer but not to the fibril. In detail, when ZAβ3W is bound to the Aβ peptide, the fluorescence intensity increased and led to a blue-shifted emission maximum λmax. Using a special simulation technique, Gruning *et al.* found a correlation between λmax and the fraction of free ZAβ3W, after which they inferred the Aβ fraction, which still remains in fibrils.[25]

In the simulation, we followed exactly the same protocol as in the experiment of Gruning *et al.*[25] that the dissociated peptide was removed from the simulation box. This can be easily implemented in simple lattice models, but it is not so in an all-atom model, where the removal of one chain requires to re-solvate a simulation box with a reduced number of water molecules. Thus, in this work, we only used a lattice model to capture the process without recycling.

Quantities used for data analysis

Fraction of fibril contacts Ω

Because the simulation started from the fibril structure (Figs. 1, 4, and 5) at $t = 0$, the number of fibril contacts, $N_{\text{fibril}}(0)$, is the largest one. The fraction of fibril contacts, which measures the β-structure, is defined as $\Omega(t) = N_{\text{fibril}}(t)/N_{\text{fibril}}(0)$. Experimentally, this quantity can be obtained by the ThT fluorescence technique.

Fraction of bound monomers Θ

Monomers that have no contact with the rest are called free monomers. The number of bound (non-free) monomers that belong to oligomers or fibrils is the difference between the total number of monomers and the number of free monomers. The concentration of non-free monomers is defined as $\Theta(t) = N_{\text{non-free}}/N$. In experiments, this quantity can be measured by the tryptophan fluorescence.[25] In the capture scenario (without recycling), a monomer detached from the aggregate is removed from the simulation box.

Free energy

To show the existence of intermediate states, we calculated the free energy as a function of fibril contacts. It is defined as follows:

$$G(N_{\text{fibril}}) = -k_B T \ln(P(N_{\text{fibril}})), \tag{2}$$

where $P(N_{\text{fibril}})$ is the population of states with N_{fibril} fibril contacts. In simulation, $P(N_{\text{fibril}}) = n(N_{\text{fibril}})/n_{\text{total}}$, where $n(N_{\text{fibril}})$ is the number of times the state with N_{fibril} fibril contacts occurs and n_{total} is the total number of sampled conformations.

The calculation of the equilibrium free energies is very time consuming since the degradation and formation of fibrils are irreversible processes. For systems with a finite number of chains, these processes are reversible but building equilibrium free energy landscapes remains computationally difficult. Therefore, we will construct nonequilibrium free energy landscapes, using Eq. (2) and all sampled snapshots including those taken before equilibration.

RESULTS

Theory

Dissociation of monomers from fibril without recycling

Logistic behavior. In the first approximation, the decay of the number of bound chains depends linearly on the number of chains, i.e., $d\Theta/dt \sim \Theta$ or $d\Theta/dt = -a\Theta$, where parameter $a > 0$ for decomposition. This equation leads to exponentially fast decay $\Theta \sim \exp(-at)$. However, as can be seen from the simulation results below (Figs. 3, 5, and 7), $\Theta(t)$ decreases much more slowly than exponential behavior at short time scales. To overcome this difficulty, we add a term that is proportional to Θ^2, leading to the following kinetics equation:

$$\frac{d\Theta}{dt} = -a\Theta + b\Theta^2, \tag{3}$$

where fitting parameter $b > 0$. Equation (3) is similar to the equation for population growth, but the sign of the right side is opposite (https://en.wikipedia.org/wiki/Logistic_function).

In our phenomenological theory, temperature is implicitly expressed through adjustable parameters. For example, we do not

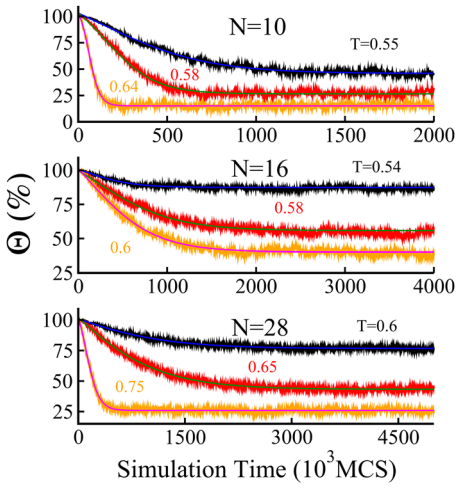

FIG. 3. Time dependence of percentage of bound monomers, $\Theta(t)$, with recycling. Color curves represent the logistic fitting [Eq. (7)] for each data set at different temperatures and N. For $N = 10$, the sets of fitting parameters (Θ_0, Θ_{eq}, $\tilde{b}$, τ) are (57.21, 45.83, 3.64×10^{-5}, 294.1), (74.25, 26.75, 9.26×10^{-5}, 121.95), and (87.61, 15.17, 3.4×10^{-4}, 29.6) for $T = 0.55$, 0.58, and 0.64, respectively. For $N = 16$, they are (14.76, 87.39, 8.26×10^{-5}, 502.5), (44.0, 55.82, 3.11×10^{-5}, 438.6), and (61.109, 40.18, 2.391×10^{-5}, 378.78) for $T = 0.54$, 0.58, and 0.60, respectively. In the $N = 28$ case, we have (24.21, 76.44, 2.301×10^{-5}, 791.4), (58.74, 43.20, 1.088×10^{-5}, 645.2), and (76.13, 25.89, 1.14×10^{-4}, 89.3) for $T = 0.60$, 0.65, and 0.75, respectively. The characteristic time τ is measured in 10^3 MCS and highlighted in blue.

know exactly the temperature dependence of the parameters a and b in Eq. (3), but we expect a to increase with temperature because degradation accelerates with an increase in temperature. The parameter b may decrease or increase with T depending on the situation (see below). In general, these parameters should be chosen in such a way that the right side of Eq. (3) is negative in order to guarantee a decrease in Θ with time. Thus, at $t = 0$, we have $b\Theta^2 - a\Theta < 0$ or $b\Theta_0/a < 1$. The larger the system, the more stable the system; hence, the parameters a and b should depend on the system size. This will be confirmed by our simulation.

Equation (3) has the exact solution

$$\Theta(t) = \frac{\Theta_0}{\tau b\Theta_0 + (1 - \tau b\Theta_0)e^{t/\tau}}, \tag{4}$$

implying that, in general, the fraction of bound chains follows logistic kinetics without recycling. Here, the parameter τ ($\tau = 1/a$) plays the role of "relaxation" time. Since degradation becomes faster with an increase in temperature, τ should decrease with an increase in T.

Single exponential kinetics. At large enough time scales, the second term in the denominator in Eq. (4) dominates over the first term and we have

$$\Theta(t) \sim \exp(-t/\tau). \tag{5}$$

We will show that this single exponential kinetics can describe the experiment of fibril degradation without recycling.[25] Namely, using a special technique that does not allow the separated monomers to reunite with the mother oligomer, it was shown that the dissociation of monomer[25] obeys a single exponential kinetics if the fraction of bound proteins becomes less than the crossover value $\Theta_{cr} \sim 90\%$.

Dissociation of monomers from fibril with recycling

When released monomers are not captured, one has to add to Eq. (3) an additional term that describes the recycling. Because the probability of recycling depends not only on the size of the parent cluster but also on the number of free monomers, this term should be proportional to $\Theta(\Theta_0 - \Theta)$. Then, Eq. (3) becomes

$$\frac{d\Theta}{dt} = -a\Theta + b\Theta^2 + c\Theta(\Theta_0 - \Theta). \tag{6}$$

Because the recycling disfavors degradation, the coefficient $c > 0$. Introducing $\tilde{a} = a - c\Theta_0$ and $\tilde{b} = b - c$, the last equation becomes identical to Eq. (3) but with the renormalized parameters $\tilde{a}$ and $\tilde{b}$ and $\Theta_0 \to \Theta_0 - \Theta_{eq}$. In other words, for the case of recycling, the dissociation of monomers from the aggregate is governed by the following logistic equation:

$$\Theta(t) = \frac{\Theta_0 - \Theta_{eq}}{\tilde{b}(\Theta_0 - \Theta_{eq})\tau + [1 - \tilde{b}(\Theta_0 - \Theta_{eq})\tau]e^{t/\tau}} + \Theta_{eq}, \tag{7}$$

where $\tau = 1/\tilde{a}$. Contrast to the case without recycling, in the $t \to \infty$ limit, the portion of bound chains approaches a nonzero equilibrium value Θ_{eq}. Equation (7) satisfies this condition and the requirement that $\Theta = \Theta_0$ at $t = 0$. Note that the parameter Θ_{eq} should depend on a, b, and c, but we do not have an analytical dependence. It can be obtained in simulation from the time dependence of $\Theta(t)$ in the limit $t \to \infty$.

Simulation results and comparison with experiment

Dissociation with recycling

Time dependence of the number of bound chains: Lattice models. Figure 3 shows the time dependence of the fraction of bound chains for $N = 10$, 16, and 28 at different temperatures. Recall that the temperature in the lattice model is implied in the Metropolis algorithm and is dimensionless as k_BT is measured in the characteristic energy ε_{HB}.[34] Simulations were carried out at $T > 0.39$, i.e., above room temperature.

In agreement with our theory, the logistic dependence [Eq. (7)] works well for all cases. As the temperature is lowered, the portion of bound monomers at large time scales becomes larger or Θ_{eq} increases. For $N = 28$, $\Theta_{eq} = 76.44\%$, 43.20%, and 25.89% for $T = 0.60$, 0.65, and 0.75, respectively. The value of Θ_{eq} for $N = 10$ and 16 at different temperatures is given in the caption of Fig. 3.

Time dependence of the fibril contacts: Lattice models. The fraction of fibril contacts, $\Omega(t)$, can be experimentally measured by the ThT fluorescence array, and it was shown that[24] its time dependence is described by a bi-exponential function,

$$\Omega(t) = \Omega_0 + \Omega_1 \exp(-t/\tau_1) + \Omega_2 \exp(-t/\tau_2). \tag{8}$$

The existence of two time scales τ_1 and τ_2 means that the fibril degradation occurs through an intermediate state. τ_1 and τ_2 describe the decay at short and large time scales, respectively. To demonstrate the existence of an intermediate state, we plot the free energy as a function of the fraction of fibril contacts for $N = 28$ and $T = 0.60$ (Fig. 4) (similar results for other systems and temperatures are not shown). For individual trajectories, we have two local maxima implying that the intermediate state occurs upon fibril dissociation. It is important to note that two local minima disappear if we average over many MC trajectories (bottom panel in Fig. 4) due to the fact that local minima/maxima of separate paths are located at different positions.

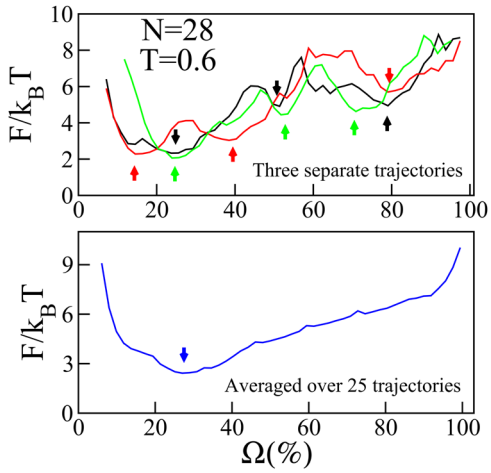

FIG. 4. Top panel: free energy as a function of the fraction of fibril contacts, obtained in three MC trajectories, for $N = 28$, $T = 0.60$. Bottom panel: the same as on the top panel, but the results were averaged over 25 trajectories. Arrows show the position of local minima.

Therefore, care must be taken when interpreting simulation data on a free energy landscape.

As can be seen from Fig. 5, in accordance with the experiment,[24] the fraction of fibril contacts is perfectly fitted to the bi-exponential function. For a given number of chains, characteristic times τ_1 and τ_2 decrease with an increase in temperature (caption of Fig. 5) since with shorter characteristic times, the degradation occurs faster. Depending on the system size and temperature, τ_2 is 1–2 orders of magnitude greater than τ_1. This result is consistent with the experiment on degradation of β2-microglobulin amyloid fibrils,[24] which showed that the off-rate constant of the second term is much greater than the first one.

Figure 6 shows the temperature dependence of the degradation rates $\kappa_{off1} = 1/\tau_1$ and $\kappa_{off12} = 1/\tau_2$. These results suggest that both rates obey the Arrhenius formula as they depend linearly on $1/T$. Using the experimental data (Fig. 3 from the work of Kardos *et al.*[24]), we can show that the degradation kinetics of $\beta 2m$ amyloid fibrils is bi-exponential (Fig. S2). Using the fitting parameters from Fig. S2, we can extract κ_{off1} and κ_{off12} and show that they also obey the Arrhenius law (Fig. S3). Thus, our simulation results are consistent with the experiment.[24]

Time dependence of the number of bound chains: All-atom model. Because the lattice model can produce artificial results due to its discrete nature, we carried out the MD simulation with the use of all-atom models with explicit water. The simulation started from the fibril-like structure of 10 truncated peptides $A\beta_{37-42}$ at T = 350 K, 375 K, and 400 K (Fig. 7). For each temperature, 10 trajectories were performed with different initial velocity fields, and the

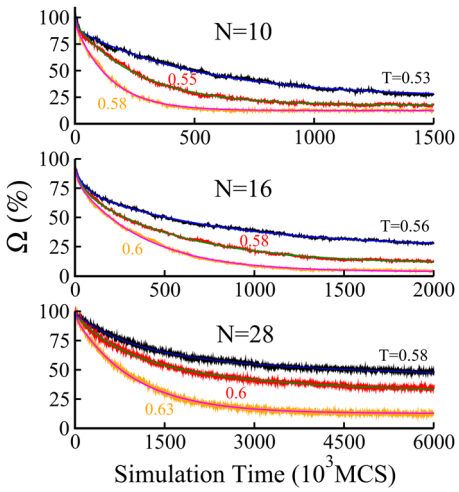

FIG. 5. Thermal degradation kinetics of three fibril structures with10, 16, and 28 polypeptide chains at different temperatures. The results were obtained using the lattice model. Smooth curves refer to the bi-exponential fit given by Eq. (8). For N = 10, the set (Ω_0, Ω_1, Ω_2, τ_1, τ_2) is (24.81, 17.65, 64.61, 8.55, 526.32), (17.29, 14.18, 76.8, 4.35,277.78), and (12.45, 13.55, 81.41, 3.73, 147.06) for T = 0.53, 0.55, and 0.58, respectively. For N = 16, we have (24.6, 17.79, 49.67, 55.56, 769.23), (10.24, 16.09, 67.79, 47.62, 588.24), and (3.68, 11.84, 77.47, 17.54, 384.61) for T = 0.56, 0.58, and 0.60, respectively. In the N = 28 case, the fitting sets are (40.95, 33.92, 23.04, 961.54, 4761.90), (30.1, 32.16, 34.85, 751.88, 2564.10), and (12.7, 5.35, 82.08, 32.26, 1000.0) for T = 0.58, 0.60, and 0.63, respectively. Here, Ω_0, Ω_1, and Ω_2 are in % and τ_1 and τ_2 are measured in 10^3 MCS.

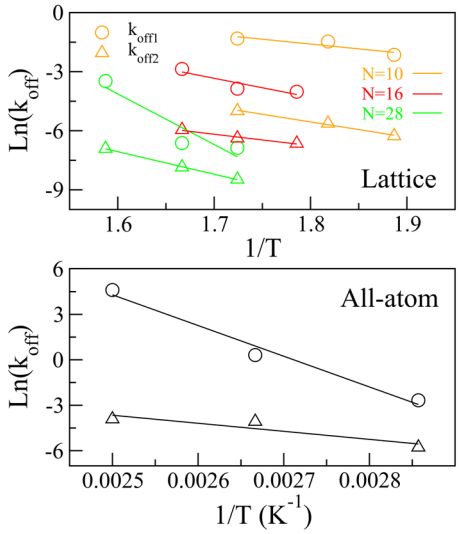

FIG. 6. Temperature dependence of the degradation rate κ_{off1} and κ_{off2}, obtained by using the lattice (upper panel) and all-atom simulation (lower panel). K_{off} is measured in $(10^3 \text{ MCS})^{-1}$.

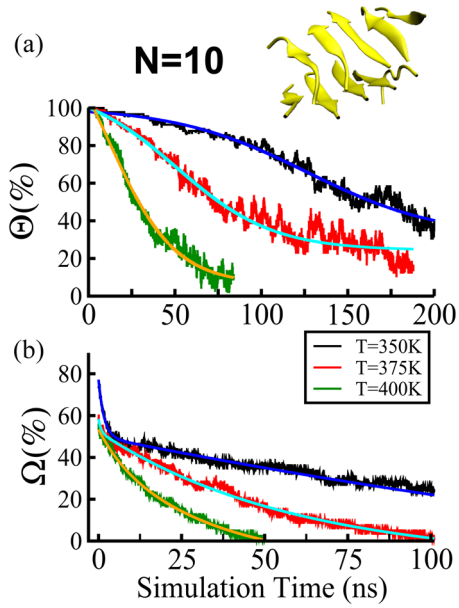

FIG. 7. Upper panel: fibril-like structure of 10 truncated peptides $A\beta_{37-42}$. This structure has 113 fibril contacts. (a) Dependence of the percentage of bound monomers $\Theta(t)$ on the simulation time without the capture of released monomers. The results were obtained using the all-atom model. The logistic fitting [Eq. (7)] was conducted for each data set at different temperatures. The sets of fitting parameters (Θ_0, Θ_{eq}, $\tilde{b}$, τ) are (72.43, 26.25, 2.9 × 10^{-4}, 45.45), (84.87, 18.94, 1.9 × 10^{-4}, 43.48), and (99.02, 6.34, 3.2 × 10^{-4}, 19.61) for T = 350 K, 375 K, and 400 K, respectively. The results were averaged over 10 MD trajectories. (b) Time dependence of the fraction of fibril contacts of N = 10 chains, $\Omega(t)$, in the all-atom simulation. Bi-exponential fits are $y = 27.58e^{-t/1.64} + 102.1e^{-t/322.6} - 52.14$ (T = 350 K), $y = 6.13e^{-t/0.73} + 62.35e^{-t/58.8} - 9.95$ (T = 375 K), and $y = 11.31e^{-t/0.01} + 53.93e^{-t/50} - 11.85$ (T = 400 K). Time t is measured in ns.

results were averaged over all trajectories. As in the lattice model, the fraction of bound chains $\Theta(t)$ obeys the logistic behavior [Eq. (7)]. We can show that the set of fitting parameters $(\tilde{b}, \tau)$ is equal to $(2.9 \times 10^{-4}, 45.5)$, $(1.9 \times 10^{-4}, 43.5)$, and $(3.3 \times 10^{-4}, 19.6)$ for T = 350 K, 375 K, and 400 K, respectively (caption of Fig. 7). The characteristic time τ, which is measured in ns, is of order of 10 ns and decreases with an increase in T as the temperature increase speeds up the degradation.

From a visual inspection, it seems that multiple exponential fits are also suitable for the time dependence of the number of bound chains. To clarify this issue, we performed exponential fits with different time scales, as shown in Fig. S4. The bi- and tri-exponential fits do not work at T = 350 K because the initial slow decay cannot be captured. This remains valid for a higher-order fit (results not shown). At T = 375, the tri-exponential works better than in the T = 350 K case, but again the initial decrease in Θ cannot be described. At T = 400 K, both logistic and single exponential fits work well. So, at sufficiently high temperatures, when the degradation is fast, a fit with multiple time scales should work.

Time dependence of the fibril contacts: All-atom model. Figure 7 shows that the portion of fibril contacts $\Omega(t)$ of 10 short peptides $A\beta_{37-42}$ is well described by the bi-exponential function, given by Eq. (8). The set of fitting parameters $(\Omega_0, \Omega_1, \Omega_2, \tau_1, \tau_2)$ are (−52.14, 27.58, 102.1, 1.64, 322.6), (−9.95, 6.13, 62.35, 0.73, 58.8), and (−11.85, 11.31, 53.93, 0.01, 50) for T = 350 K, 375 K, and 400 K, respectively (caption of Fig. 7). The characteristic time τ_1 decreases from 1.64 ns to 0.01 ns and τ_2 decreases from 322.6 ns to 50 ns as the temperature increases from 350 K to 400 K, implying that the degradation is very sensitive to temperature. It can be expected that at sufficiently high temperatures, the time dependence of the fibril contacts can be described by a single exponential because the initial stage becomes so short that $\tau_1 \to 0$.

Fibril contacts decay faster than the number of bound chains: All-atom simulation of 5Aβ_{17-42}. From the lattice simulation, it can be seen that with an increase in temperature, $\Omega(t)$ decreases faster than $\Theta(t)$ (Figs. 3 and 5). For N = 10 and at T = 0.55 and $t = 5 * 10^5$ MCS, $\Theta(t) \approx 67\%$, which is higher than $\Omega(t) \approx 29\%$. For N = 16 and T = 0.60, after $t = 1.5 * 10^6$ MCS, we have $\Theta(t) \approx 49\%$, but $\Omega(t)$ drops to 8.5%. This is also true for the all-atom model with 10Aβ_{37-42} (Fig. 7), where at t = 25 ns, $\Theta(t) \approx 96.7$, 87.5%, and 52.2%, whereas $\Omega(t) \approx 42.5\%$, 32.1%, and 15.7% for T = 350 K, 375 K, and 400 K, respectively.

However, the simplicity of the lattice model and the shortness of the chains studied in the all-atom model can affect our main conclusion, prompting us to study the degradation of the fibril structure of longer sequences using the all-atom model. We performed the MD simulation starting from the fibril-like structure of five $A\beta_{17-42}$ chains (PDB ID: 2BEG[39]) and using the AMBER force filed 99SB. The 2BEG structure has 184 fibril contacts. Figure 8 shows the time dependence of the fraction of fibril contacts at 300 K. This fraction (or the β-content) rapidly decreases according to the exponential law. Although both fits work well for simulation data as indicated by the high correlation levels (R = 0.97 and 0.99 for the single and bi-exponential fits, respectively), only the bi-exponential fit captures the initial stage of the decay process. In the bi-exponential fit, the off-rate constant of the first term is about 22 times greater than the second one. This result is in qualitative agreement with the exponential behavior observed in experiments on the dissociation of the β 2m amyloid fibril in the elevated temperature region[24] as well as at the ambient temperature.[25]

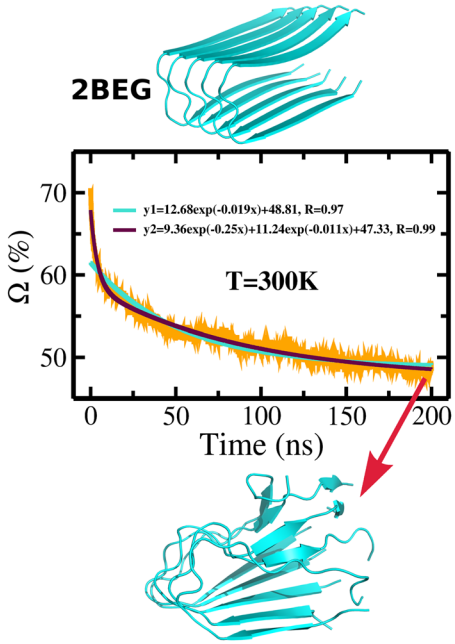

FIG. 8. Time dependence of fibril contacts of 2BEG at T = 300 K. The results were averaged over MD 20 trajectories of 200 ns. Shown is the fibril structure 2BEG from PDB (upper panel) and one of the last snapshots in the simulation (lower panel).

At t = 200 ns, the fraction of fibril contacts $\Omega(t)$ falls below 50% but $\Theta(t)$ remains equal to 100% as none of the chains was dissociated from the fibril (Fig. 8). This clearly demonstrates that the reduction of $\Omega(t)$ is much faster than $\Theta(t)$ and this behavior cannot be fitted to the logistic function [Eq. (7)]. This is the major difference between two quantities.

Dissociation without recycling

Time dependence of the number of bound chains: Lattice models. To study the degradation without recycling, MC simulation was started with fibril conformations shown in Fig. 2 for N = 10, 16, and 28, but, as in the experiment by Gruning *et al.*,[25] we removed any released chain from the box, not allowing it to rejoin the mother aggregate. To get good statistics, hundreds of MC trajectories were generated using different random seed numbers. The results were averaged over all trajectories.

Figure 9 shows the time dependence of the fraction of bound chains in lattice models with N = 10, 16, and 28 in the capture scenario. For all cases and three temperatures, the curves are perfectly fitted to Eq. (3), implying that the thermal degradation obeys the logistic behavior. Because τ controls the degradation rate, it decreases as the temperature increases (caption of Fig. 9). For example, in the N = 16 case, we have $\tau = 892.9 \times 10^3$, 396.8×10^3,

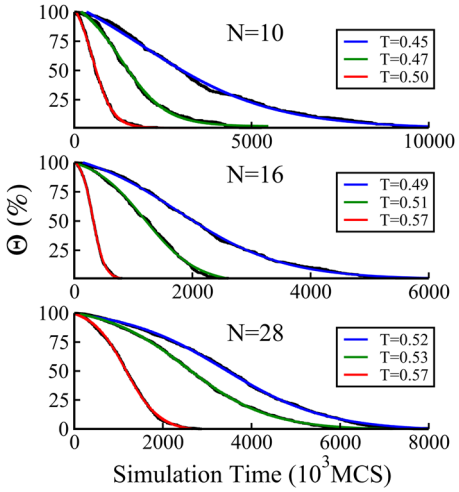

FIG. 9. Dependence of the fraction of bound monomers Θ on the simulation time in the capture scenario for N = 10, 16, and 28 and three temperatures. Black curves refer to the raw data. The color curves refer to the logistics fit [Eq. (3)]. For N = 10, sets of fitting parameters (Θ_0, b, τ) are (105.0, 3.83 × 10^{-6}, 1852.8), (101.7, 1.383 × 10^{-5}, 632.9), and (101.9, 3.006 × 10^{-5}, 285.7) for T = 0.45, 0.47, and 0.50, respectively. In the N = 16 case, we obtained (101.98, 9.69 × 10^{-6}, 892.9), (98.18, 2.45 × 10^{-5}, 396.8), and (100.78, 9.508 × 10^{-5},101.0) for T = 0.49, 0.51, and 0.57, respectively. For N = 28, we have (98.48, 0.924 × 10^{-6}, 1098.9), (99.69, 1.051 × 10^{-5}, 909.1), and (98.19, 2.45 × 10^{-5}, 400.0) for T = 0.52, 0.53, and 0.57, respectively. The characteristic time τ is measured in 10^3 MCS and highlighted in blue.

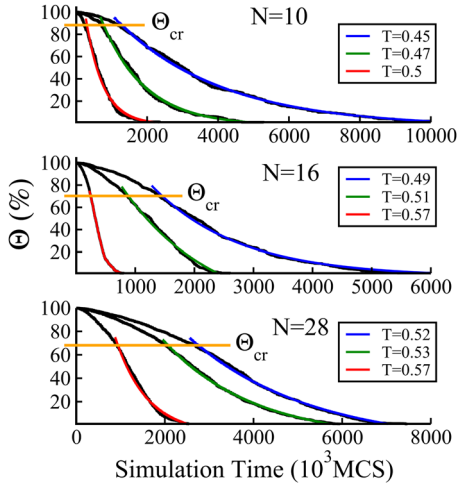

FIG. 10. Data are the same as in Fig. 6, but we show the single exponential fit after $\Theta(t)$ reached the crossover value Θ_{cr}, noted by the orange straight line. Here, Θ_{cr} = 87%, 70%, and 67% for N = 10, 16, and 28, respectively. The blue, dark green, and red curves represent an exponential fit by equation $\Theta = \Theta_0 * \exp(-x/\tau) + \Theta_1$. For N = 10, the parameter set (Θ_0, τ, Θ_1) is (140.54, 2857, −3.01), (170.89, 1220, −2.11), and (166.44, 500, −0.79) for T = 0.45, 0.47, and 0.5, respectively. For N = 16, we have (194.13, 1538, −2.13), (196.58, 1471, −39.67), and (260.85, 208, −6.8) for T = 0.49, 0.51, and 0.57, respectively. For N = 28, we have (230.74, 2778, −17.8), (222.89, 2041, −12.41), and (280.22, 714, −7.66) for T = 0.52, 0.53, and 0.57, respectively. The characteristic time τ is measured in 10^3 MCS and highlighted in blue.

and 101 × 10^3 MCS for T = 0.49, 0.51, and 0.57, respectively. A similar result was obtained for N = 10 and 28.

We can show that in the case when the capture of released chains is allowed, the time dependence of the fibril contacts can be represented using a bi-exponential function [Eq. (8)].

Crossover from logistic to single-exponential kinetics. Initially, when the rigidity of the fibril is still high, $\Theta(t)$ slowly decreases (Fig. 10), but after reaching the crossover value Θ_{cr}, the degradation becomes fast and the kinetics can be described by the single exponential function (Fig. 10). Θ_{cr} depends on the number of chains and temperature, but as a rule, the smaller the N and the higher the T, the larger the Θ_{cr}. This is because as the number of chains is increased or the temperature is lowered, it becomes increasingly difficult to fit the data into single exponential function. For all temperatures studied, we obtained Θ_{cr} = 87%, 70%, and 67% for N = 10, 16, and 28, respectively (Fig. 10). Restricting to data with $\Theta \le \Theta_{cr}$, we get a good single exponential fit for all cases studied. This result agrees with the experiment,[25] which shows that single exponential kinetics works for Θ_{cr} < 90%. As expected, for a given N, the relaxation time τ [Eq. (4)] decreases with the temperature. For example, in the N = 28 case, τ = 2778 × 10^3, 2041 × 10^3, and 714 × 10^3 MCS for T = 0.52, 0.53, and 0.57, respectively (Fig. 10).

Temperature and size dependence of the parameters of the phenomenological theory

The fitting parameters a, b, $\tilde{a}$, $\tilde{b}$, and Θ_0 (parameter c is just intermediate and not involved in the final formula of the theory) in our phenomenological theory [Eqs. (4) and (7)] can be obtained using microscopic theory. However, this issue is beyond the scope of the present paper. Here, we extract their temperature dependence from the lattice and all-atom simulation (Fig. S5). In all cases, a and $\tilde{a}$ increase with T because they are the main factors that control the intensification of dissociation with an increase in temperature. The behavior of b and $\tilde{b}$ is more complicated as they can increase as well as decrease with T (Fig. S5). In the all-atom models with recycling and the lattice models without recycling, the parameter Θ_0 grows with temperature, but in the lattice model with recycling, its temperature dependence is not monotonic.

Since the fibril stability depends on the system size, the fitting parameters should depend on the number of chains (Fig. S5). In the lattice model, for a given temperature, a and $\tilde{a}$ decrease with an increase in N. As expected, the dependence of b and $\tilde{b}$ on the system size is not monotonic.

Exponential vs logistic kinetics from the free energy perspective

We have shown that the decay of the number of fibril contacts can be described by a bi-exponential function, while the slower time dependence of the number of dissociated chains is subordinate to the logistic function. Since the kinetic properties are determined by thermodynamics, it is worth understanding the difference between the two kinetics in terms of free energy landscapes.

The bi-exponential kinetics is associated with the existence of one intermediate in the free energy profile plotted as a function of the fraction of fibril contacts (Fig. 4). Because the logistic kinetics is

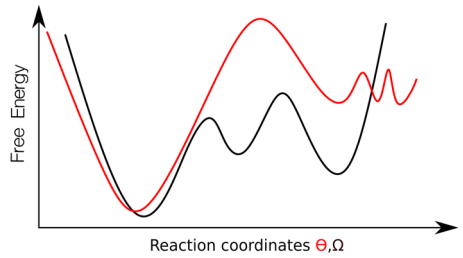

FIG. 11. Schematic plots for free energy landscapes plotted as a function of the fraction of fibril contacts Ω (black) and the fraction of bound chains Θ (red). Bi-exponential kinetics of Ω is associated with two maxima (black curve), while logistic behavior of Θ is due to a pronounced maximum and a rough free energy profile at the initial stage (red curve).

related to the time dependence of the number of bound chains, we plot the free energy as a function the fraction of bound chains Θ for the lattice model with $N = 28$ at $T = 0.75$ (Fig. S6). For a sufficiently large Θ (initial stage), the presence of shallow local minima can be considered as a roughness of free energy that led to a slow decay in the logistic behavior. On a large time scale, the logistic kinetics becomes exponential due to the existence of a global maximum of free energy (Fig. S6).

The free energy profiles that are responsible for the difference between two kinetics are depicted in Fig. 11. For bi-exponential kinetics, the corresponding free energy, plotted as a function of the fraction of fibril contacts Ω, has two pronounced maxima separating ordered and disordered states. In the case of logistic behavior, there is only one barrier that controls fast kinetics at sufficiently large time scales, while the initial slow decay of the fraction of coupled chains is related to the roughness of free energy.

CONCLUSION

We have developed a theory to describe the temperature-induced degradation of protein aggregates. Our theory is phenomenological since the temperature dependence is accounted in accordance with the fitting constants rather than from physical insights. It is shown that the decrease in the number of bound chains, which can be measured by using the tryptophan fluorescence technique, is represented by a logistic function. This contrasts sharply with the bi-exponential kinetics of fibril contacts or beta content, which can be experimentally monitored using the ThT fluorescence array. Logistic kinetics occurs in both cases with and without recycling of released chains. The main difference between the logistic and bi-exponential behavior is that in the first case, the decrease in the corresponding quantity is slower than in the second case. The number of connected chains decreases with time more slowly than the fibril content because to separate a chain from an aggregate, one needs to break more inter-chain contacts than to spoil beta-sheets.

We explored the difference between bi-exponential and logistic kinetics in terms of free energy. It was shown that the bi-exponential behavior is associated with the existence of two maxima in the free energy profile, plotted as a function of the fraction of fibril contacts. If the proportion of bound chains Θ is used as the reaction coordinate, then the free energy has one global maximum and shallow traps at large values of Θ. Such free energy led to logistic behavior.

Our lattice and all-atom simulations support the bi-exponential kinetics observed in the experiment of Kardos *et al.*, who measured the ThT fluorescence signal characterizing the content of fibrils.[24] Studying the free energy profile, we showed that this behavior is due to the existence of intermediate states. Using the tryptophan fluorescence technique to monitor the fraction of released proteins, it was found[25] that the degradation kinetics is described by a single exponential function if recycling is not allowed. We show that a single exponential behavior occurs if we ignore the slow dynamics when the concentration of bound chains exceeds the crossover value Θ_{cr}. For the entire time interval, logistic kinetics should take place regardless of whether we capture the released polypeptide chains or not. It would be interesting to check our prediction of logistic behavior experimentally.

SUPPLEMENTARY MATERIAL

See the supplementary material for Fig. S1—temperature dependence of the fraction of fibril contacts $\langle Q(T)\rangle$of the lattice monomer; Fig. S2—experimental data, obtained by Goto's group, for thermal dissociation of β2m amyloid fibrils at different temperatures; Fig. S3—temperature dependence of two experimental degradation rates k_{off1} and k_{off2}, extracted from the bi-exponential fits shown in Fig. S2; Fig. S4—dependence of percentage of bound monomers $\Theta(t)$ on the simulation time without the capture of released monomers and multiple exponential fits; Fig. S5—temperature dependence of parameters of the phenomenological theory; and Fig. S6—free energy of the lattice model with $N = 28$ chains plotted as a function the fraction of bound chains Θ for three trajectories at $T = 0.75$.

AUTHOR'S CONTRIBUTIONS

N.T.C. and P.D.L. contributed equally to this work.

ACKNOWLEDGMENT

This work was supported by the Narodowe Centrum Nauki in Poland (Grant No. 2015/19/B/ST4/02721) and the Department of Science and Technology of Ho Chi Minh City, Vietnam. The allocation of CPU time at the supercomputer center TASK in Gdansk and PLGrid infrastructure (Poland) is highly appreciated.

REFERENCES

[1] J. Hardy and D. J. Selkoe, Science **297**(5580), 353–356 (2002).
[2] J. Kang, H. G. Lemaire, A. Unterbeck, J. M. Salbaum, C. L. Masters, K.-H. Grzeschik, G. Multhaup, K. Beyreuther, and B. J. Muller-Hill, Nature **325**, 733–736 (1987).
[3] C. Haass and D. J. Selkoe, Nat. Rev. Mol. Cell Biol. **8**, 101–112 (2007).
[4] J. Nasica-Labouze, P. H. Nguyen, F. Sterpone, O. Berthoumieu, N. V. Buchete, S. Cote, A. De Simone, A. J. Doig, P. Faller, A. Garcia, A. Laio, M. S. Li, S. Melchionna, N. Mousseau, Y. G. Mu, A. Paravastu, S. Pasquali, D. J. Rosenman, B. Strodel, B. Tarus, J. H. Viles, T. Zhang, C. Y. Wang, and P. Derreumaux, Chem. Rev. **115**(9), 3518–3563 (2015).
[5] J. Brange, L. Andersen, E. D. Laursen, G. Meyn, and E. Rasmussen, J. Pharm. Sci. **86**(5), 517–525 (1997).
[6] D. Hamada and C. M. Dobson, Protein Sci. **11**, 2417–2426 (2002).

[7]N. Hirota-Nakaoka, H. Kazuhiro, N. Hironobu, and G. Yuji, J. Biochem. **134**(1), 159–164 (2003).
[8]J. Murali and R. Jayakumar, J. Struct. Biol. **150**(2), 180–189 (2005).
[9]T. Narimoto, K. Sakurai, A. Okamoto, E. Chatani, M. Hoshino, K. Hasegawa, H. Naiki, and Y. Goto, FEBS Lett. **576**(3), 313–319 (2004).
[10]H. Wille and S. B. Prusiner, Biophys. J. **76**, 1048–1062 (1999).
[11]W. Dzwolak, Biochim. Biophys. Acta **1764**(3), 470–480 (2006).
[12]D. Foguel and J. L. Silva, Biochemistry **43**(36), 11361–11370 (2004).
[13]F. Meersman and C. M. Dobson, Biochim. Biophys. Acta **1764**(3), 452–460 (2006).
[14]J. Torrent, C. Balny, and R. Lange, Protein Pept. Lett. **13**, 271–277 (2006).
[15]T. Kawasaki, J. Fujioka, T. Imai, K. Torigoe, and K. Tsukiyama, Lasers Med. Sci. **29**(5), 1701–1707 (2014).
[16]M. H. Viet, P. Derreumaux, M. S. Li, C. Roland, C. Sagui, and P. H. Nguyen, J. Chem. Phys. **143**(15), 155101 (2015).
[17]A. Arora, C. Ha, and C. B. Park, Protein Sci. **13**(9), 2429–2436 (2004).
[18]U. Baxa, P. D. Ross, R. B. Wickner, and A. C. Steven, J. Mol. Biol. **339**, 259–264 (2004).
[19]L. Bousset, F. Briki, J. Doucet, and R. Melki, J. Struct. Biol. **141**, 132–142 (2003).
[20]J. Dubois, A. A. Ismail, S. L. Chan, and Z. Ali-Khan, Scand. J. Immunol. **49**, 376–380 (1999).
[21]S. V. Litvinovich, S. A. Brew, S. Aota, S. K. Akiyama, C. Haudenschild, and K. C. Ingham, J. Mol. Biol. **280**, 245–258 (1998).
[22]B. Morel, L. Varela, and F. Conejero-Lara, J. Phys. Chem. B **114**, 4010–4019 (2010).
[23]K. Sasahara, H. Naiki, and Y. Goto, J. Mol. Biol. **352**, 700–711 (2005).
[24]J. Kardos, A. Micsonai, H. Pal-Gabor, E. Petrik, L. Gráf, J. Kovács, Y.-H. Lee, H. Naiki, and Y. Goto, Biochemistry **50**(15), 3211–3220 (2011).
[25]C. S. R. Gruning, S. Klinker, M. Wolff, M. Schneider, K. Toksoz, A. N. Klein, L. Nagel-Steger, D. Willbold, and W. Hoyer, J. Biol. Chem. **288**, 37104–37111 (2013).
[26]W. Hoyer, C. Grönwall, A. Jonsson, S. Ståhl, and T. Härd, Proc. Natl. Acad. Sci. U. S. A. **105**, 5099–5104 (2008).
[27]L. M. Luheshi, W. Hoyer, T. P. de Barros, I. van Dijk Hard, A. C. Brorsson, B. Macao, C. Persson, D. C. Crowther, D. A. Lomas, S. Stahl, C. M. Dobson, and T. Hard, PLoS Biol. **8**(3), e1000334 (2010).
[28]D. K. Klimov and D. Thirumalai, Structure **11**(3), 295–307 (2003).
[29]P. H. Nguyen, M. S. Li, G. Stock, J. E. Straub, and D. Thirumalai, Proc. Natl. Acad. Sci. U. S. A. **104**(1), 111–116 (2007).
[30]P. D. Q. Huy, Q. V. Vuong, G. La Penna, P. Faller, and M. S. Li, ACS Chem. Neurosci. **7**(10), 1348–1363 (2016).
[31]S. Mitternacht, I. Staneva, T. Hard, and A. Irback, J. Mol. Biol. **410**(2), 357–367 (2011).
[32]L. Nagel-Steger, M. C. Owen, and B. Strodel, ChemBioChem **17**(8), 657–676 (2016).
[33]W. H. Zheng, M. Y. Tsai, M. C. Chen, and P. G. Wolynes, Proc. Natl. Acad. Sci. U. S. A. **113**(42), 11835–11840 (2016).
[34]M. S. Li, D. K. Klimov, J. E. Straub, and D. Thirumalai, J. Chem. Phys. **129**, 175101 (2008).
[35]M. S. Li, N. T. Co, G. Reddy, C.-K. Hu, J. E. Straub, and D. Thirumalai, Phys. Rev. Lett. **105**, 218101 (2010).
[36]N. T. Co and M. S. Li, J. Chem. Phys. **137**(9), 095101 (2012).
[37]N. T. Co, C. K. Hu, and M. S. Li, J. Chem. Phys. **138**(18), 185101 (2013).
[38]M. S. Li and M. Cieplak, Phys. Rev. E **59**(1), 970–976 (1999).
[39]T. Lührs, C. Ritter, M. Adrian, D. Riek-Loher, B. Bohrmann, H. Doeli, D. Schubert, and R. Riek, Proc. Natl. Acad. Sci. U. S. A. **102**, 17342–17347 (2005).
[40]A. T. Petkova, W.-M. Yau, and R. Tycko, Biochemistry **45**(2), 498–512 (2006).
[41]A. K. Paravastu, R. D. Leapman, W. M. Yau, and R. Tycko, Proc. Natl. Acad. Sci. U. S. A. **105**, 18349–18354 (2008).
[42]I. Bertini, L. Gonnelli, C. Luchinat, J. Mao, and A. Nesi, J. Am. Chem. Soc. **133**(40), 16013–16022 (2011).
[43]H. A. Scheidt, I. Morgado, S. Rothemund, and D. Huster, J. Biol. Chem. **287**, 2017–2021 (2012).
[44]J. X. Lu, W. Qiang, W. M. Yau, C. D. Schwieters, S. C. Meredith, and R. Tycko, Cell **154**, 1257–1268 (2013).
[45]M. A. Walti, F. Ravotti, H. Arai, C. G. Glabe, J. S. Wall, A. Bockmann, P. Guntert, B. H. Meier, and R. Riek, Proc. Natl. Acad. Sci. U. S. A. **113**(34), E4976–E4984 (2016).
[46]L. Gremer, D. Scholzel, C. Schenk, E. Reinartz, J. Labahn, R. B. G. Ravelli, M. Tusche, C. Lopez-Iglesias, W. Hoyer, H. Heise, D. Willbold, and G. F. Schroder, Science **358**(6359), 116 (2017).
[47]D. A. Pearlman, D. A. Case, J. W. Caldwell, W. S. Ross, T. E. Cheatham III, S. DeBolt, D. Ferguson, G. Seibel, and P. Kollman, Comput. Phys. Commun. **91**(1-3), 1–41 (1995).
[48]D. A. Case, T. E. Cheatham, T. Darden, H. Gohlke, R. Luo, K. M. Merz, A. Onufriev, C. Simmerling, B. Wang, and R. J. Woods, J. Comput. Chem. **26**(16), 1668–1688 (2005).
[49]V. Hornak, R. Abel, A. Okur, B. Strockbine, A. Roitberg, and C. Simmerling, Proteins: Struct., Funct., Bioinf. **65**(3), 712–725 (2006).
[50]W. L. Jorgensen, J. Chandrasekhar, J. D. Madura, R. W. Impey, and M. L. Klein, J. Chem. Phys. **79**(2), 926–935 (1983).
[51]W. F. van Gunsteren, S. R. Billeter, A. A. Eising, P. H. Hunenberger, P. Kruger, A. E. Mark, W. R. P. Scott, and I. G. Tironi, *Biomolecular Simulation: The GROMOS96 Manual and User Guide* (Vdf Hochschulverlag AG an der ETH Zurich, Zurich, 1996).
[52]T. T. Nguyen, M. H. Viet, and M. S. Li, Sci. World J. **2014**, 536084.
[53]R. W. Hockney, S. P. Goel, and J. Eastwood, J. Comput. Phys. **14**(2), 148–158 (1974).
[54]J.-P. Ryckaert, G. Ciccotti, and H. J. C. Berendsen, J. Comput. Phys. **23**(3), 327–341 (1977).
[55]X. W. Wu and B. R. Brooks, Chem. Phys. Lett. **381**(3-4), 512–518 (2003).
[56]T. Darden, D. York, and L. Pedersen, J. Chem. Phys. **98**(12), 10089–10092 (1993).